nature photonics

LETTERS

PUBLISHED ONLINE: 1 FEBRUARY 2016 | DOI: 10.1038/NPHOTON.2015.274

Ghost imaging in the time domain

Piotr Ryczkowski[1], Margaux Barbier[1], Ari T. Friberg[2], John M. Dudley[3] and Goëry Genty[1]*

Ghost imaging is a novel technique that produces the image of an object by correlating the intensity of two light beams, neither of which independently carries information about the shape of the object[1,2]. Ghost imaging has opened up new perspectives to obtain highly resolved images[3], even in the presence of noise and turbulence[4]. Here, by exploiting the duality between light propagation in space and time[5], we demonstrate the temporal analogue of ghost imaging. We use a conventional fast detector that does not see the temporal 'object' to be characterized and a slow integrating 'bucket' detector that does see the object but without resolving its temporal structure. Our experiments achieve temporal resolution at the picosecond level and are insensitive to the temporal distortion that may occur after the object. The approach is scalable, can be integrated on-chip, and offers great promise for dynamic imaging of ultrafast waveforms.

Ghost imaging uses correlation measurement between light transmitted through (or reflected by) an object and the spatially resolved intensity pattern of the incident light to reconstruct the ghost image of the original object[1]. The principle of spatial ghost imaging is illustrated in Fig. 1a. The beam from a light source with a spatially random intensity pattern is divided between two paths. In one arm (test), the random incident light directly illuminates the object with the scattered light collected by a single-pixel bucket detector, which produces only a spatially integrated signal. In the second arm (reference), the incident light does not see the object at all, but the random fluctuations in the beam are measured as a function of spatial position with a high-resolution charge-coupled device (CCD) camera. Neither of the detectors alone can produce an image of the object, but by correlating the two measurements from the bucket and high-resolution detectors over multiple intensity patterns produced by the source, the object appears like a ghost in the focus plane of the camera. The essential nature of ghost imaging lies in the mutual spatial correlation of the two beams, which may be quantum or classical. Various light sources can be used, including spatially entangled photon sources[2,6–9], classical light sources[2,10–15] or structured light fields programmed by a spatial light modulator to minimize the number of measurements in the time series to obtain an accurate representation of the object[16].

Many propagation effects in optics first seen in the spatial domain have subsequently been observed in time by exploiting space–time duality—the correspondence between the diffraction of a light beam and the dispersive propagation of a short optical pulse[17–19]. Recently, this duality has successfully enabled major advances in the processing of time-varying signals including all-optical magnification of ultrafast data rates by a thousand-fold[20,21], all-optical correlation[5], real-time detection of single-shot spectra at speeds of hundreds of megahertz[22], or temporal cloaking[23]. It has also been suggested theoretically[24] and numerically[25] that this duality may allow the transposition of the concept of ghost imaging to the temporal domain. Here, we confirm this proposal experimentally, demonstrating how intensity correlation measurements from a temporally fluctuating light source allow retrieval of a rapidly varying temporal object that modulates the amplitude of the transmitted or reflected light.

We implement temporal ghost imaging using an optical fibre-based system (shown in Fig. 1b). The random intensity fluctuations of a laser diode replace the beam with a randomly fluctuating transverse intensity pattern, and the temporal intensity modulation of the incident light field imposed by an ultrafast optical modulator replaces the scattering from a spatial object. In this sense, the 'random illumination' used in ghost imaging arises from the intrinsic randomness in the temporal fluctuations of the light emitted by the laser diode, a quasi-continuous multimode laser operating at $\lambda = 1{,}547$ nm. The bandwidth is $\Delta\lambda = 0.6$ nm, resulting in random intensity fluctuations with a characteristic time $\tau_c = \lambda^2/(c\Delta\lambda) \approx 13$ ps, where c is the speed of light in vacuum. At the output of the source, the intensity is equally divided between the test and reference arms with a 50/50 fibre coupler that replaces the beamsplitter in the spatial set-up. In the reference arm, the temporal fluctuations of the source are measured with a 25 GHz photodiode and a 18 GHz real-time oscilloscope, which results in an effective fluctuation time of $\tau_c^{\mathrm{eff}} = 55$ ps. Multiple series of intensity fluctuations measured from the reference arm and recorded over a 2 ns time window are plotted in Fig. 2. One can clearly observe the random fluctuations of the intensity with an effective characteristic time of ~50 ps. We can also see that the intensity of the source averaged over a large series of consecutive 2 ns segments is constant, which ensures that the retrieved ghost image is directly proportional to the object[24] (see also Methods). In the test arm, the temporal object is a bit sequence generated by an ultrafast electro-optic modulator (EOM) driven by a 10 Gb s^{-1} pulse pattern generator that temporally modulates ('scatters') the randomly fluctuating light (see Methods). The light transmitted through the object is detected by a slow photodiode with 5 ns response time, which is too slow to resolve the temporal structure of the bit sequence.

The normalized intensity correlation function $C(t)$ (that is, the ghost image) calculated over a series of time signals measured simultaneously from both arms is defined by

$$C(t) = \frac{\langle \Delta I_{\mathrm{ref}}(t) \Delta I_{\mathrm{test}} \rangle_N}{\sqrt{\langle [\Delta I_{\mathrm{ref}}(t)]^2 \rangle_N \langle [\Delta I_{\mathrm{test}}]^2 \rangle_N}} \quad (1)$$

Here, $I_{\mathrm{ref}}(t)$ represents the time-resolved intensity measurement from the reference arm at time t, and I_{test} is the integrated intensity from the test arm. $\langle\ \rangle_N$ denotes the ensemble average over a series of N realizations and $\Delta I = I - \langle I \rangle_N$. Figure 3 shows the ghost image obtained from a series of $N = 80{,}000$ realizations where the temporal intensity fluctuations of the light source follow a random pattern in each of the realizations. The agreement with the direct image of the object measured with the fast detector is remarkable. Specifically, the temporal object (the transmission of the EOM driven by the bit sequence) is precisely reproduced both in terms of duration and amplitude.

[1]Optics Laboratory, Tampere University of Technology, PO Box 692, FI 33101, Tampere, Finland. [2]Department of Physics and Mathematics, University of Eastern Finland, PO Box 111, FI 80101, Joensuu, Finland. [3]Institut FEMTO-ST, UMR 6174 CNRS–Université de Franche-Comté, Besançon, France.
*e-mail: goery.genty@tut.fi

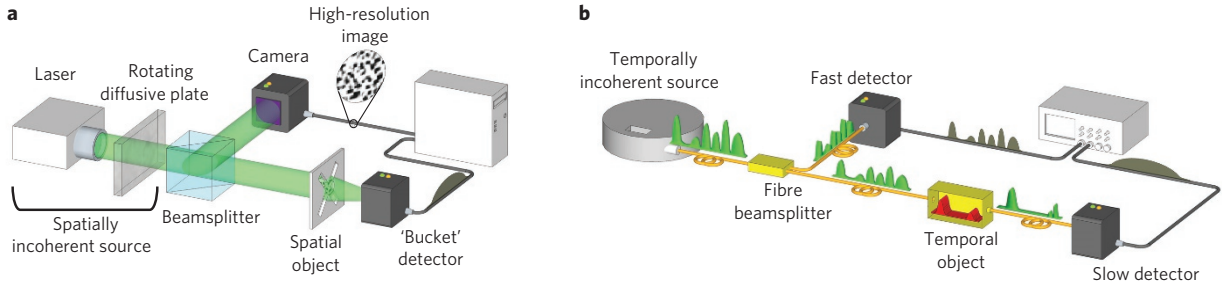

Figure 1 | Comparison of spatial and temporal ghost imaging experimental set-ups. a, Spatial set-up. **b**, Temporal set-up.

The performance of the ghost imaging system can be characterized by (1) the temporal resolution and (2) the signal-to-noise ratio (SNR). The temporal resolution directly corresponds to the effective fluctuation time (that is, the upper value between the coherence time of the source and the response time of the fast detector/oscilloscope; see Methods), which must then be shorter than the object variations that one wants to resolve. The noise in the measurement mainly arises from the standard error of the correlation function calculated from a finite number of realizations, and the SNR is given by[26]

$$\mathrm{SNR}(t) = \frac{C(t)\sqrt{N}}{1 - C^2(t)} \qquad (2)$$

assuming that the noise contribution from the detectors is negligible. The SNR is therefore expected to increase with the number of realizations and this is shown in Fig. 4a–d (see Supplementary Movie 1 for a full evolution of the ghost image as a function of the number of realizations). Note that the amplitude of the ghost image should be independent of the number of measurements, which can be readily observed in the figure. For a fixed number of realizations, the SNR can be improved by increasing the effective fluctuation time of the source. In practice, this can be done in two different ways, depending on which parameter determines the value of τ_c^{eff}: either by increasing the coherence time of the source or by decreasing the fast detector bandwidth. As a rule of thumb, to obtain a ghost image at fast acquisition rates, yet with a high temporal resolution and optimum SNR, the effective fluctuation time should be equal to half of the fastest time variations that one wants to resolve in the object (Nyquist criterion). For the 100 ps bits that constitute the object here, the effective fluctuation time for optimum SNR and acquisition time is then 50 ps. Lower values may improve the temporal resolution at the expense of the SNR, and higher values will result in the opposite. Ghost images recorded for a fixed number of measurements ($N = 5{,}000$) with the detection bandwidth in the reference arm decreasing from 18 to 2 GHz (and thus the effective fluctuation time increasing from 55 to 500 ps) are shown in Fig. 4e–h. One can clearly see how the SNR is improved as the effective fluctuation time is increased, but that this improvement occurs at the expense of temporal resolution in the ghost image.

Ghost imaging is inherently insensitive to the distortion that may occur between the object and the bucket detector. This remarkable particularity has attracted considerable attention in the spatial domain, with the possibility of performing high-resolution imaging even in the presence of a strong scattering medium or atmospheric turbulence, when any direct measurement would result in a poor-quality image. This also applies in the time domain, and we demonstrate that the technique allows distortions experienced by the modulated light field after the temporal object to be overcome. For this purpose, a 29 m multimode fibre is inserted after the EOM, which strongly distorts the bit pattern. The results in Fig. 5 clearly show how the intermodal dispersion accumulated in the multimode fibre severely distorts a direct measurement of the temporal object performed with a fast detector. However, when the ghost imaging technique is used, the distortion is washed out and has no influence on the quality of the ghost image. More generally, ghost imaging in the time domain allows compensation for arbitrary distortion experienced by a temporal object provided that the integrated transmitted intensity does not vary over the total acquisition time.

These experiments represent the first demonstration of ghost imaging in the time domain. Using an all-fibre set-up and a laser source with random intensity fluctuations, our results illustrate how an ultrafast temporal object with structure on the scale of 10 Gb s^{-1} can be measured with ~50 ps temporal resolution without directly detecting the object. The technique can be adapted to the detection of all-optical data streams by modulating the temporal fluctuations of the light source through, for example, four-wave mixing in

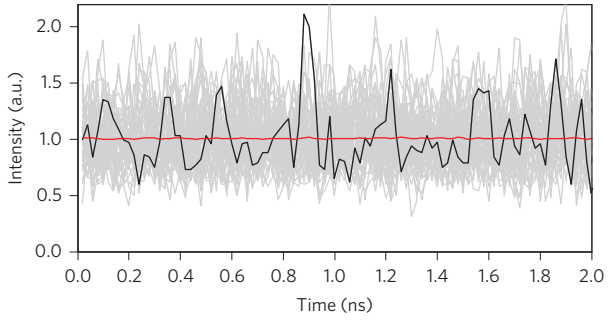

Figure 2 | Measured intensity fluctuations of the multimode laser source. A single realization (black) is shown together with 50 other realizations (grey). The average intensity of 5,000 realizations is shown as a red line.

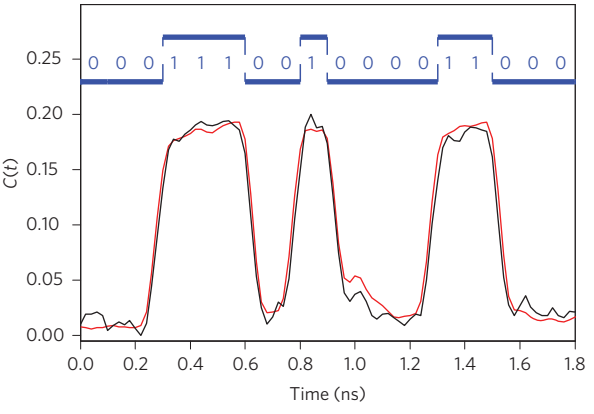

Figure 3 | Comparison of ghost image and direct image measured with the fast detector. Ghost image, black; direct image, red. The bandwidth of the detection is 18 GHz, corresponding to an effective fluctuation time of 55 ps. The number of realizations in the measurement series for the ghost image is $N = 80{,}000$. The blue line and 0/1 numbers represent the bit sequence used to create the temporal object.

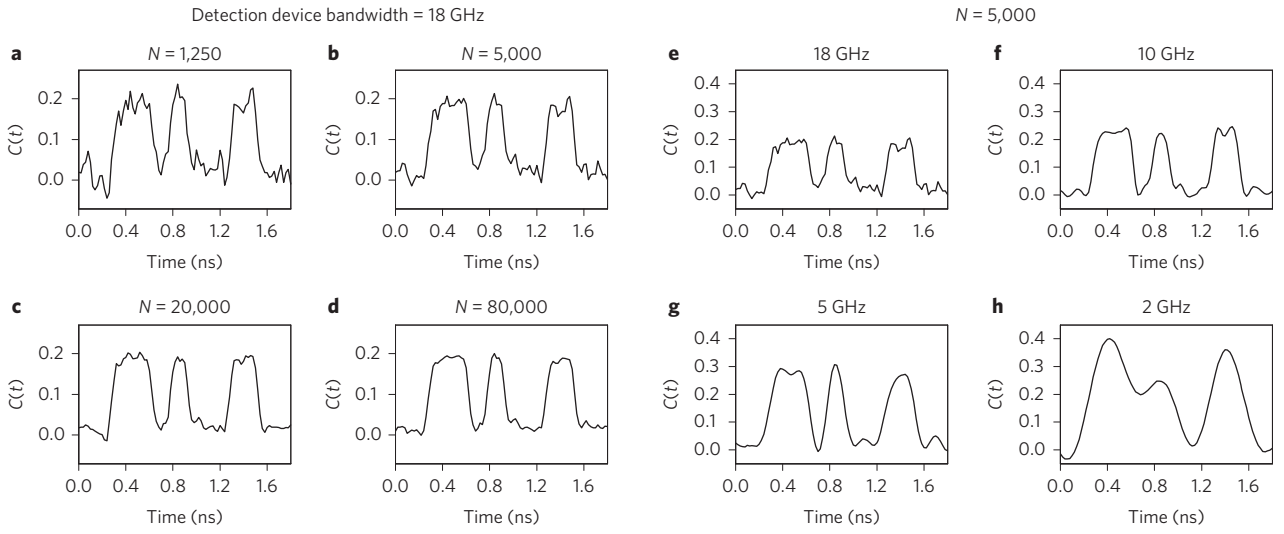

Figure 4 | Ghost image as a function of number of realizations and effective fluctuation time. a–d, The number of realizations N increases from 1,250 to 80,000. **e–h**, The effective fluctuation time τ_c^{eff} increases from 55 to 500 ps, as indicated. The temporal object is identical to that in Fig. 3.

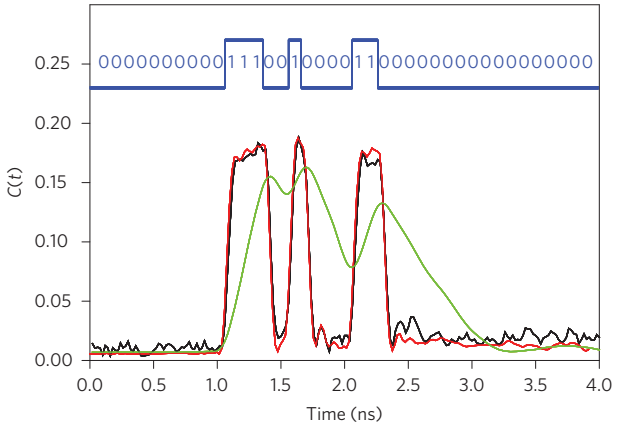

Figure 5 | Comparison of ghost image and direct image in the presence of strong dispersion experienced by the object when a multimode fibre is added between the EOM and the detector. Ghost image, black; direct image, green. For comparison, the direct image obtained without the multimode fibre is also shown in red. Both direct measurements are performed with the fast detector. The bandwidth of the detection is equal to 18 GHz, corresponding to an effective fluctuation time of 55 ps. The number of realizations in the measurement series for the ghost image is $N = 100{,}000$. The blue line and 0/1 numbers represent the bit sequence used to create the temporal object.

a nonlinear fibre. The system is scalable to any data rate and shape by adapting the coherence time of the source. Adjusting the fast detector bandwidth and number of distinct measurements allows for optimizing the measurement speed and SNR. We also emphasize that a quantum version of the temporal ghost imaging system can be implemented using entangled photon pairs. The set-up can also be modified to include a time lens[27] in the reference arm and thereby magnify the ghost image[24]. Our results open novel perspectives for dynamic imaging of ultrafast waveforms when the waveform has been severely distorted by the transmission medium, in the presence of high noise or low signal strength, and we anticipate applications in communications, remote sensing and ultrafast spectroscopy.

Methods

Methods and any associated references are available in the online version of the paper.

Received 13 May 2015; accepted 15 December 2015; published online 1 February 2016

References

1. Erkmen, B. I. & Shapiro, J. H. Ghost imaging: from quantum to classical to computational. *Adv. Opt. Photon.* **2,** 405–450 (2010).
2. Bennink, R. S., Bentley, S. J., Boyd, R. W. & Howell, J. C. Quantum and classical coincidence imaging. *Phys. Rev. Lett.* **92,** 033601 (2004).
3. Ferri, F. *et al.* High-resolution ghost image and ghost diffraction experiments with thermal light. *Phys. Rev. Lett.* **94,** 183602 (2005).
4. Meyers, R. E., Deacon, K. S. & Shih, Y. Turbulence-free ghost imaging. *Appl. Phys. Lett.* **98,** 111115 (2011).
5. Salem, R., Foster, M. A. & Gaeta, A. L. Application of space–time duality to ultrahigh-speed optical signal processing. *Adv. Opt. Photon.* **5,** 274–317 (2013).
6. Klyshko, D. N. A simple method of preparing pure states of an optical field, of implementing the Einstein–Podolsky–Rosen experiment, and of demonstrating the complementarity principle. *Sov. Phys. Usp.* **31,** 74–85 (1988).
7. Klyshko, D. N. Combine EPR and two-slit experiments: interference of advanced waves. *Phys. Lett. A* **132,** 299–304 (1988).
8. Pittman, T. B., Shih, Y. H., Strekalov, D. V. & Sergienko, A. V. Optical imaging by means of two-photon quantum entanglement. *Phys. Rev. A* **52,** R3429 (1995).
9. Abouraddy, A. F., Saleh, B. E. A., Sergienko, A. V. & Teich, M. C. Role of entanglement in two-photon imaging. *Phys. Rev. Lett.* **87,** 123602 (2001).
10. Bennink, R. S., Bentley, S. J. & Boyd, R. W. 'Two-photon' coincidence imaging with a classical source. *Phys. Rev. Lett.* **89,** 113601 (2002).
11. Scarcelli, G., Berardi, V. & Shih, Y. Can two-photon correlation of chaotic light be considered as correlation of intensity fluctuations? *Phys. Rev. Lett.* **96,** 063602 (2006).
12. Meyers, R., Deacon, K. S. & Shih, Y. Ghost-imaging experiment by measuring reflected photons. *Phys. Rev. A* **77,** 041801 (2008).
13. Shirai, T., Setälä, T. & Friberg, A. T. Ghost imaging of phase objects with classical incoherent light. *Phys. Rev. A* **84,** 041801 (2011).
14. Zhang, C., Guo, S., Cao, J., Guan, J. & Gao, F. Object reconstitution using pseudo-inverse for ghost imaging. *Opt. Express* **22,** 30063–30073 (2014).
15. Karmakar, S., Meyers, R. & Shih, Y. Ghost imaging experiment with sunlight compared to laboratory experiment with thermal light. *Proc. SPIE* **8518,** 851805 (2012).
16. Sun, B. *et al.* 3D computational imaging with single-pixel detectors. *Science* **330,** 844–847 (2015).
17. Tournois, P. *Analogie optique de la compression d'impulsions. C. R. Acad. Sci. III* **258,** 3839 (1964).
18. Kolner, B. H. & Nazarathy, M. Temporal imaging with a time lens. *Opt. Lett.* **14,** 630–632 (1989).
19. Kolner, B. H. Space–time duality and the theory of temporal imaging. *IEEE J. Quantum Electron.* **30,** 1951–1963 (1994).
20. Foster, M. A. *et al.* Silicon-chip-based ultrafast optical oscilloscope. *Nature* **456,** 81–84 (2008).
21. Schröder, J. *et al.* Aberration-free ultra-fast optical oscilloscope using a four-wave mixing based time-lens. *Opt. Commun.* **283,** 2611–2614 (2010).
22. Solli, D. R., Herink, G., Jalali, B. & Ropers, C. Fluctuations and correlations in modulation instability. *Nature Photon.* **6,** 463–468 (2012).
23. Fridman, M., Farsi, A., Okawachi, Y. & Gaeta, A. L. Demonstration of temporal cloaking. *Nature* **481,** 62–65 (2012).

24. Shirai, T., Setälä, T. & Friberg, A. T. Temporal ghost imaging with classical non-stationary pulsed light. *J. Opt. Soc. Am. B* **27,** 2549–2555 (2010).
25. Chen, Z., Li, H., Li, Y., Shi, J. & Zeng, G. Temporal ghost imaging with a chaotic laser. *Opt. Eng.* **52,** 076103 (2013).
26. Soper, H. E. On the probable error of the correlation coefficient to a second approximation waveforms. *Biometrika* **9,** 91–115 (1913).
27. Salem, R. *et al.* Optical time lens based on four-wave mixing on a silicon chip. *Opt. Lett.* **33,** 1047–1049 (2008).

Acknowledgements

G.G. and A.T.F. acknowledge support from the Academy of Finland (projects 267576 and 268480). J.M.D. acknowledges support from ERC project MULTIWAVE. The Optoelectronics Research Centre, Tampere University of Technology is also thanked for the loan of the pulse pattern generator.

Author contributions

G.G. and A.T.F. conceived the original idea. P.R. and M.B. constructed the experimental set-up and conducted all the experiments. G.G. designed the experiments and supervised the project. P.R., M.B., J.M.D. and G.G. performed the data analysis. All authors discussed the results and contributed to writing the manuscript.

Additional information

Supplementary information is available in the online version of the paper. Reprints and permissions information is available online at www.nature.com/reprints. Correspondence and requests for materials should be addressed to G.G.

Competing financial interests

The authors declare no competing financial interests.

Methods

In the present experiments, the object was created by a zero-chirp 10 GHz bandwidth electro-optic modulator (Thorlabs LN81S-FC) driven by a pulse pattern generator (Advantest D3186). The 10 GHz clock signal was generated by a microwave signal generator (Rohde & Schwarz SMR20), resulting in bits of 100 ps duration. The detector in the test arm was a 1.2 GHz InGaAs photodiode (Thorlabs DET01CFC). Its response was integrated over 5 ns, such that the effective bandwidth was equal to 0.2 GHz only. The detector in the reference arm measuring the intensity fluctuations of the source was a 25 GHz InGaAs photodiode (UPD-15-IR2-FC Alphalas). The oscilloscope was a 20 GHz, 50 Gsamples/s real-time oscilloscope (DSA72004 Tektronix). Accounting for the electrical cables that were used, the actual bandwidth was estimated to be 18 GHz. The object was repeated periodically with a period of 50 ns. As a result, the data acquisition time required for 100,000 realizations was only on the order of 5 ms.

The coherence time τ_c of the source corresponds to the characteristic time of its intensity fluctuations. If the response time τ_{det} of the fast detection device (detector + oscilloscope) in the reference arm is shorter than τ_c (that is, if the detection device can resolve the fluctuations of the source), then the temporal resolution of the ghost imaging process is equal to τ_c and objects details that are shorter than τ_c cannot be resolved. On the other hand, if τ_{det} is longer than τ_c (as is the case in our experiments), then the characteristic time of the intensity fluctuations that are effectively recorded by the detection device is $\tau_c^{eff} \sim \tau_{det}$ ($>\tau_c$) and the temporal resolution of the ghost imaging process is thus given by τ_{det}. In other words, the temporal resolution is set by τ_c^{eff}, which is the maximum value between τ_c and τ_{det}.

To obtain a direct correspondence between the correlation and the original object it is important that the intensity fluctuations averaged over the number of realizations is constant over the measurement time window of a single realization. This condition is generally fulfilled in the case of a quasi-continuous-wave light source but does not hold if one uses a pulsed light source. In this latter case, the temporal object would be distorted by the time variation of the average intensity (or average pulse shape)[24].

All the fibres were SMF-28 patch cords of 1 m length with a dispersion parameter of 18 ps nm^{-1} km^{-1} at 1,550 nm, except the multimode fibre used to add distortion, which was a 29 m fibre (Thorlabs FG105LCA). Because the SMF-28 fibres were short, dispersion accumulated during propagation from the source to the fast detector on the one hand and from the source to the object (EOM) on the other, was negligible. No temporal lens was therefore needed to perform the imaging process, and the magnification factor between the object and the ghost image was simply equal to 1. This situation is equivalent in the spatial case to the near-field regime as described in ref. 11.